

Mining higher-order triadic interactions

Anthony Baptista,^{1,2} Marta Niedostatek,¹ Jun Yamamoto,³ Ben MacArthur,^{2,4,5}
Jürgen Kurths,^{6,7} Ruben Sanchez Garcia,^{2,4} and Ginestra Bianconi^{1,2}

¹*School of Mathematical Sciences, Queen Mary University of London, London, E1 4NS, United Kingdom*

²*The Alan Turing Institute, The British Library, London, NW1 2DB, United Kingdom*

³*Department of Network and Data Science, Central European University, Vienna 1100, Austria*

⁴*School of Mathematical Sciences, University of Southampton, Southampton SO17 1BJ, United Kingdom*

⁵*Faculty of Medicine, University of Southampton, Southampton SO17 1BJ, United Kingdom*

⁶*Potsdam Institute for Climate Impact Research, 14473 Potsdam, Germany*

⁷*Institute of Physics, Humboldt University of Berlin, 12489 Berlin, Germany*

Complex systems often present higher-order interactions which require us to go beyond their description in terms of pairwise networks. Triadic interactions are a fundamental type of higher-order interaction that occurs when one node regulates the interaction between two other nodes. Triadic interactions are a fundamental type of higher-order networks, found in a large variety of biological systems, from neuron-glia interactions to gene-regulation and ecosystems. However, triadic interactions have been so far mostly neglected. In this article, we propose a theoretical principle to model and mine triadic interactions from node metadata, and we apply this framework to gene expression data finding new candidates for triadic interactions relevant for Acute Myeloid Leukemia. Our work reveals important aspects of higher-order triadic interactions often ignored, which can transform our understanding of complex systems and be applied to a large variety of systems ranging from biology to the climate.

I. INTRODUCTION

Higher-order networks [1–5] are key to capture many-body interactions present in complex systems. Inferring higher-order interactions from real, pairwise network datasets is recognised as one of the central challenges in the study of higher-order networks [2]. Despite the increasing attention given to the inference of higher-order interactions [6–14], the detection of triadic interactions, which are prevalent in a wide variety of complex systems, has been addressed only in few works [15–17] and remains an important scientific challenge.

Triadic interactions [18] are a fundamental type of signed higher-order interaction. A triadic interaction occurs when one or more nodes regulate the interaction between two other nodes. The regulator nodes may either enhance or inhibit the interaction between the other two nodes. Triadic interactions are known to be important in various systems such as ecosystems [19–21] where one species can regulate the interaction between two species, neuronal networks [22] where glial cells regulate synaptic transmission between neurons thereby regulating brain information processing, and gene regulation networks [16, 23] where a modulator can promote or silence the interaction between a transcription factor and a target gene. Despite evidence of triadic interactions in specific disciplines (neuroscience, ecology, molecular biology), the relevance of triadic interactions as a universal type of higher-order interactions with a well-defined mathematical definition has only recently been recognised [18, 24–27].

In this article, we explore the fundamental dynamical

properties of networks with triadic interactions between continuous variables. We formulate a general model of networks with triadic interactions, and propose an information theory framework and the Triaction algorithm that is able to mine triadic interactions from data. The Triaction algorithm leverages the induced variability of the mutual information between a pair of variables when conditioned on a third regulatory variable. Using our method, we show that triadic interactions are important in gene-expression data where genes can be involved in ‘trigenic’ processes [28]. We apply the Triaction algorithm to a gene-expression network data, and are able to detect known interactions as well as propose a set of new candidate interactions that can then be validated experimentally.

II. TRIADIC INTERACTIONS

A triadic interaction occurs when one or more nodes modulate (or regulate) the interaction between two other nodes, either positively or negatively. A triadic interaction network is a heterogeneous network composed of a structural network and a regulatory network encoding triadic interactions (Figure 1). The structural network $G_S = (V, E_S)$ is formed by a set V of N nodes and a set E_S of L edges. The regulatory network $G_R = (V, E_S, E_R)$ is a signed bipartite network with one set nodes given by V (the nodes of the structural network), and another set of nodes given by E_S (edges of the structural network) connected by the regulatory interactions E_R of cardinality $|E_R| = \hat{L}$. The signed regulatory network can be encoded as an $L \times N$ matrix K where $K_{\ell i} = 1$ if node i activates the structural edge ℓ , $K_{\ell i} = -1$ if node i inhibits the

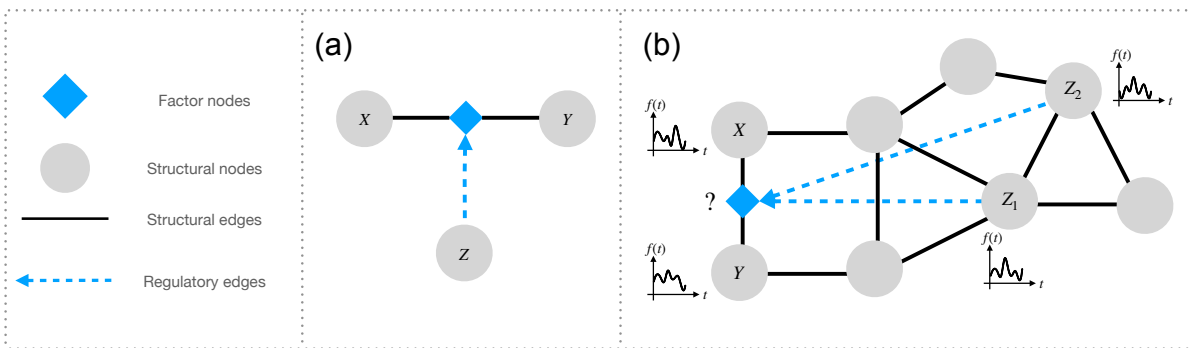


Figure 1. (Panel a) A triadic interaction occurs when a node, here shown as Z , regulates either positively or negatively the interaction between two other nodes X and Y connected in the structural network by an edge. The node Z is also called a *regulator node*. This edge can be conceptualised as a *factor node* (shown here as a cyan diamond). (Panel b) A network with triadic interactions can be seen as a network of networks formed by a simple structural network and by a bipartite regulatory network between regulator nodes and regulated edges (factor nodes).

structural edge ℓ and $K_{\ell i} = 0$ otherwise. If $K_{\ell i} = 1$, then the node i is called a positive regulator of the edge ℓ , and if $K_{\ell i} = -1$, then the node i is called a negative regulator of the edge ℓ . It's worth noting that node $i \in V$ cannot serve as both a positive and negative regulator for the same edge ℓ at the same time. However, node i can act as a positive regulator for edge ℓ while simultaneously functioning as a negative regulator for a different edge, denoted as ℓ' , where $\ell' \neq \ell$.

III. THE CONTINUOUS TRIADIC INTERACTION MODEL

Here we formulate a general synthetic dynamical model for a network with triadic interactions between continuous variables. This model acts as a test benchmark to validate the Triaction algorithm that we propose to detect triadic interactions from continuous data. We assume that each node i of the network is associated with a dynamical variable $X_i \in \mathbb{R}$, and that the dynamical state of the entire network is encoded in the state vector $\mathbf{X} = (X_1, X_2, \dots, X_N)^T$. The topology of the structural network is encoded in the graph Laplacian matrix \mathbf{L} with elements

$$L_{ij} = \begin{cases} -a_{ij}J & \text{if } i \neq j, \\ \sum_j a_{ij}J & \text{if } i = j, \end{cases} \quad (1)$$

where $\mathbf{A} = (a_{ij})$ is the adjacency matrix of the network, and $J > 0$ is a coupling constant. In the absence of triadic interactions, we assume that the dynamics of the network is associated with a Gaussian process implemented as the Langevin equation

$$d\mathbf{X} = -\frac{\delta\mathcal{H}}{\delta\mathbf{X}} + \Gamma\boldsymbol{\eta}(t) \quad (2)$$

associated with the Hamiltonian

$$\mathcal{H} = \frac{1}{2}\mathbf{X}^\top(\mathbf{L} + \alpha\mathbf{I})\mathbf{X}, \quad (3)$$

where $\Gamma > 0$, $\alpha > 0$, and $\boldsymbol{\eta}(t)$ indicates an uncorrelated Gaussian noise with

$$\langle \eta_i(t)\eta_j(t') \rangle = \delta_{ij}\delta(t-t'). \quad (4)$$

The resulting Langevin dynamics is given by

$$d\mathbf{X} = -(\mathbf{L} + \alpha\mathbf{I})\mathbf{X}dt + \Gamma d\boldsymbol{\eta}(t). \quad (5)$$

We remark that the Hamiltonian \mathcal{H} has a minimum for $\mathbf{X} = \mathbf{0}$, and its depth increases as the value of α increases. In a deterministic version of the model ($\Gamma = 0$), the effect of the structural interactions will not be revealed at stationarity. However, the Langevin dynamics with $\Gamma > 0$ encodes for the topology on the network. Indeed, at stationarity the correlation matrix $C_{ij} = \mathbb{E}((X_i - \mathbb{E}(X_i))(X_j - \mathbb{E}(X_j)))$ is given by

$$C_{ij} = \frac{\Gamma^2}{2}[\mathbf{L} + \alpha\mathbf{I}]_{ij}^{-1}. \quad (6)$$

In other words from the correlation matrix between the dynamical variable it is possible to infer the Laplacian, and hence the connectivity of the network. We now introduce triadic interactions in the model. As explained earlier, triadic interactions occur when one or more nodes modulate the structural interactions between another two nodes. To incorporate triadic interactions into the network dynamics, we modify the definition of the Laplacian operator present in the Langevin equation. Namely, we consider the Langevin dynamics

$$d\mathbf{X} = -(\mathbf{L}^{(T)} + \alpha\mathbf{I})\mathbf{X}dt + \Gamma d\boldsymbol{\eta}(t), \quad (7)$$

obtained from Eq.(2) by substituting the graph Laplacian \mathbf{L} with the *triadic Laplacian* $\mathbf{L}^{(T)}$ whose elements are

given by

$$L_{ij}^{(T)} = \begin{cases} -a_{ij}J_{ij}(\mathbf{X}) & \text{if } i \neq j, \\ \sum_{k=1}^N a_{ik}J_{ik}(\mathbf{X}) & \text{if } i = j. \end{cases} \quad (8)$$

Moreover, we assume that the coupling constants $J_{ij}(\mathbf{X})$ are determined by a perceptron-like model that considers all the regulatory nodes of the link $\ell = [i, j]$ and the sign of the regulatory interactions. Specifically, if $\sum_{k=1}^N K_{\ell k}X_k \geq \hat{T}$ then we set $J_{ij} = w^+$; if instead $\sum_{k=1}^N K_{\ell k}X_k < \hat{T}$ then we set $J_{ij} = w^-$, with $w_+, w_- \in \mathbb{R}_+$ and $w_+ > w_-$. In other words, we set

$$J_{ij}(\mathbf{X}) = w_- + (w_+ - w_-)\theta\left(\sum_{k=1}^N K_{\ell k}X_k - \hat{T}\right), \quad (9)$$

where $\theta(\cdot)$ is the Heaviside function ($\theta(x) = 1$ if $x \geq 0$ and $\theta(x) = 0$ if $x < 0$). Note that, in the presence of the triadic interactions, the stochastic differential equation (7) is not associated with any Hamiltonian, and a stationary state of the dynamics is not guaranteed, making this dynamical process significantly more complex than the original Langevin dynamics in Eq.(2). This generic model of triadic interactions is related to the recently proposed model [27] to capture information propagation in multilayer networks but does not make use of a multilayer representation of the data. Moreover the model is significantly different from models of higher-order interactions previously proposed in the context of consensus dynamics [29, 30] or contagion dynamics [31, 32]. Indeed, in our framework, triadic interactions between continuous variables are not reducible to standard higher-order interactions because they involve the modulation of the interaction between pair of nodes. Moreover, this modulation of the interaction is not dependent on the properties of the interacting nodes and their immediate neighbours such as in [29, 30] or in the machine learning attention mechanism [33]. On the contrary, the modulation of the interaction is determined by a third regulatory node or a larger set of regulatory nodes encoded in the regulatory network

Our model of triadic interactions, therefore, shows that triadic interactions are higher-order interactions that cannot be reduced to pairs of pairwise interactions. An important problem that then arises is whether such interactions can be mined (extracted) from real data. To address this issue, we will formulate a new algorithm – that we call the Triaction algorithm – to identify triadic interactions from data, and we will test its performance on the data generated from the model described above.

IV. MINING TRIADIC INTERACTIONS

A. The Triaction algorithm

We propose the Triaction algorithm (see Figure 2) to mine triadic interactions among triples of nodes. To simplify the notation we will use the letters X, Y, Z to indicate both nodes as well as their corresponding dynamical variables.

Given a structural edge between nodes X and Y , our goal is to determine a confidence level for the existence of a triadic interaction involving an edge between node X and node Y with respect to a potential regulator node Z . Specifically, we aim to determine whether the node Z regulates the edge between node X and node Y , given the dynamical variables X, Y and Z associated with these nodes. To do so, given a time series associated with node Z , we first sort the Z -values, and define P bins in terms of z -percentiles, chosen in such a way that each bin comprises the same number of data points (ranging in our analyses from 30 to 100). We indicate with z_m the quantile of Z corresponding to the percentile m/P . Therefore, each bin m indicates data in which Z ranges in the interval $[z_m, z_{m+1})$. We indicate with $\mu(x|z_m), \mu(y|z_m)$ and $\mu(x, y|z_m)$ the probability density of the variable X, Y and the joint probability density of the variables X and Y in each m -th bin.

A triadic interaction occurs when the node Z affects the strength of the interaction between the other two nodes X and Y . Consequently, our starting point is to consider the mutual information between the dynamical variables X and Y conditional to the specific value of the dynamical variable Z . We thus consider the quantity $MIz(m) = MI(X, Y|Z = z_m)$ defined as

$$MIz(m) = \int dx \int dy \mu(x, y|z_m) \log \left(\frac{\mu(x, y|z_m)}{\mu(x|z_m)\mu(y|z_m)} \right).$$

In order to estimate this quantity, we rely on non-parametric methods based on entropy estimation from k -nearest neighbors [34–36]. For each triple of nodes, we visualize the mutual information MIz computed as a function of the z -th quantiles z_m and fit this function with a decision tree comprising r splits.

In the absence of triadic interactions, we expect MIz to be approximately constant as a function of the z -th quantiles z_m , while, in the presence of triadic interactions, we expect this quantity to vary significantly as a function of z_m . The discretized conditional mutual information CMI between X and Y conditioned on Z can be written as

$$CMI_{X,Y;Z} = \sum_{m=0}^{P-1} p(z_m)MIz(m) = \langle MIz \rangle, \quad (10)$$

where $p(z_m) = 1/P$ indicates the probability that the Z value falls in the m -th bin. This quantity is known to indicate important information about the interaction

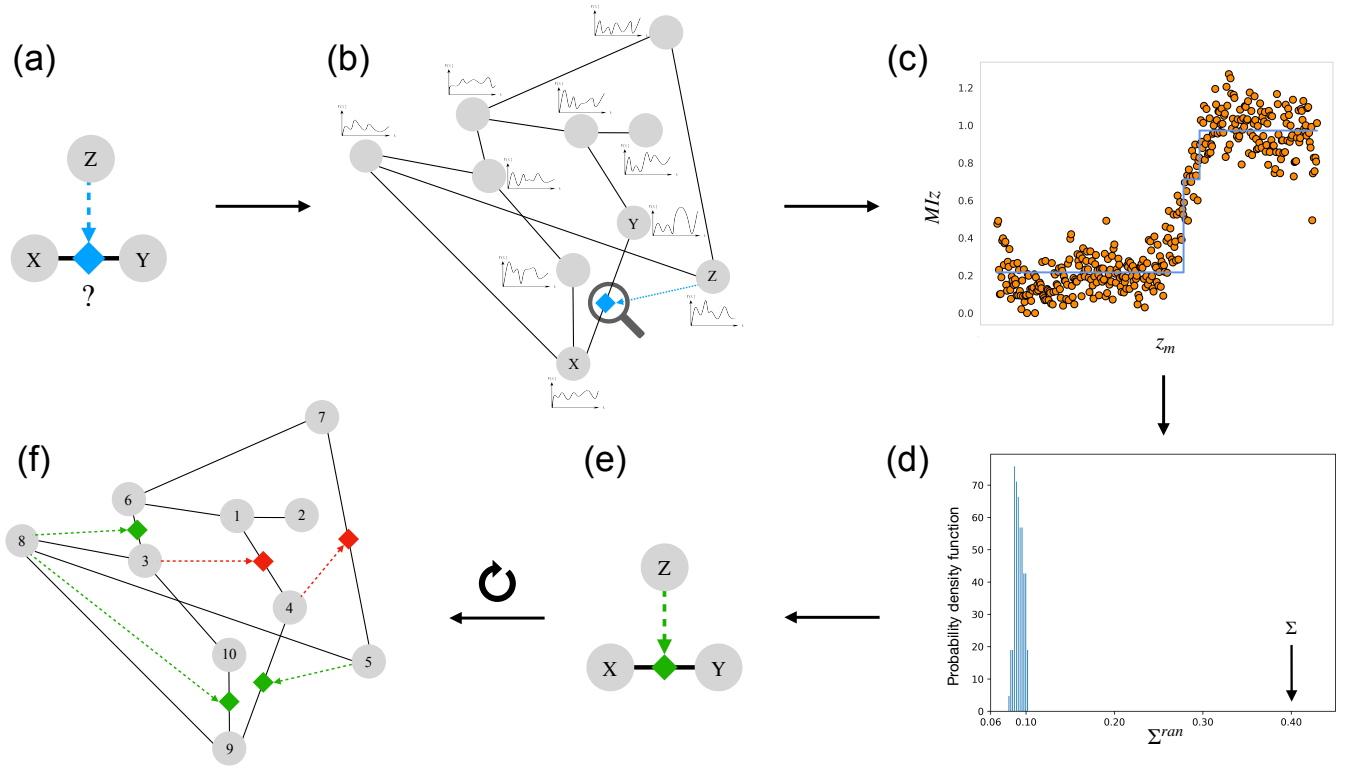


Figure 2. The Triaction algorithm identifies triples of nodes X , Y , and Z involved in a putative triadic interaction, starting from the knowledge of the structural network and the dynamical variables associated with its nodes. For each putative triple of nodes involved in a triadic interaction (panel (a)) which belong to a network whose structure and dynamics is known (panel (b)), we study the functional behavior of the conditional mutual information MIz (panel (c)), and assess the significance of the observed modulations of MIz with respect to a null model (panel (d)). Given a predetermined confidence level, we can use these statistics to identify significant triadic interactions (panel (e)). This procedure can be extended to different triples of the network, thereby identifying the triadic interactions present in it (panel (f)).

between the nodes X and Y when combined with the information coming from the mutual information MI given by

$$MI_{X,Y} = \int dx \int dy \mu(x,y) \log \left(\frac{\mu(x,y)}{\mu(x)\mu(y)} \right),$$

where $\mu(x)$, $\mu(y)$ are the probability density functions for X and Y and $\mu(x,y)$ is the joint probability density functions of the variables X and Y . In particular, true interactions between X and Y are typically associated with both high mutual information MI and high conditional mutual information CMI.

The conditional mutual information CMI, however, is not sensitive to variations in MIz and does not therefore provide the information needed to detect triadic interactions. In order to overcome this limitation, we define the following three quantities that measure how much the mutual information between X and Y conditioned on $Z \in [z_m, z_{m+1})$ changes as z_m varies. Specifically we consider:

- (1) the standard deviation Σ of MIz , defined as

$$\Sigma = \sqrt{\sum_{m=0}^{P-1} p(z_m) [MIz(m) - \langle MIz \rangle]^2}; \quad (11)$$

- (2) the difference T between the maximum and minimum value of MIz , given by

$$T = \max_{m=0, \dots, P-1} |MIz(m) - \langle MIz \rangle|; \quad (12)$$

- (3) the largest absolute difference T_n of MIz between consecutive bins, i.e.

$$T_n = \max_{m=0, \dots, P-2} |\Delta_m(MIz)|, \quad (13)$$

where

$$\Delta_m(MIz) = MIz(m) - MIz(m+1).$$

The quantities Σ , T , and T_n collectively measure the strength of the triadic interaction under question and can thus be used to mine triadic interactions in real

data. In order to assess the significance of the putative triadic interaction, we compare the observed values of these variables to a null model obtained by shuffling the Z values, to give \mathcal{N} randomization of the data, i.e. we use surrogate data for testing [37, 38]. In order to determine if the observed values are significant, we compute the scores Θ_Σ , Θ_T , Θ_{T_n} given by

$$\begin{aligned}\Theta_\Sigma &= \frac{\Sigma - \mathbb{E}(\Sigma^{ran})}{\sqrt{\mathbb{E}((\Sigma^{ran})^2) - (\mathbb{E}(\Sigma^{ran}))^2}}, \\ \Theta_T &= \frac{T - \mathbb{E}(T^{ran})}{\sqrt{\mathbb{E}((T^{ran})^2) - (\mathbb{E}(T^{ran}))^2}}, \\ \Theta_{T_n} &= \frac{T_n - \mathbb{E}(T_n^{ran})}{\sqrt{\mathbb{E}((T_n^{ran})^2) - (\mathbb{E}(T_n^{ran}))^2}},\end{aligned}\quad (14)$$

and the p -values

$$\begin{aligned}p_\Sigma &= \mathbb{P}(\Sigma^{ran} > \Sigma), \\ p_T &= \mathbb{P}(T^{ran} > T), \\ p_{T_n} &= \mathbb{P}(T_n^{ran} > T_n).\end{aligned}\quad (15)$$

Note that since we consider \mathcal{N} realizations of the null model, we cannot estimate probabilities smaller than $1/\mathcal{N}$. Therefore, if in our null model we observe no value of Σ^{ran} larger than the true data Σ , we set the conservative estimate $p_\Sigma = 1/\mathcal{P}$. A similar procedure is applied also to p_T and p_{T_n} .

For each structural edge between node X and node Y we can, of course, mine for triadic interactions involving different regulators nodes Z . To compare predictions, we rank these interactions from most to least likely via lowest to the highest p -value, or alternatively from highest to lowest Θ value and select the top k ranked triadic interactions, or those above a predetermined significance level.

As we will discuss below, the algorithm performs well on our synthetic model. However, this algorithm focuses exclusively on triples of nodes, and so neglects potentially important network effects. Thus, the algorithm is expected to give better results for triples of nodes in which Z is not significantly correlated with either X or Y .

B. Validation of the Triaction algorithm on the triadic interaction model

To demonstrate the efficacy of the Triaction algorithm we consider a single network (see Figure 4(a)) of $N = 10$ nodes, $L = 12$ edges and $\hat{L} = 5$ single triadic interactions (each formed by a single node regulating a single edge) on top of which we consider the triadic dynamical model proposed in Sec. III.

Simulations of Eq. (7) on this network show a strong dependence of $MIz(m)$ on m for the triples of nodes involved in triadic interactions, with greater significance for smaller values of α . Figure 3 shows evidence of this

interesting dynamical behavior in the case of a positive regulatory interaction. The function $MIz(m)$ is fitted with a decision tree with two splits. In this way, three different intervals of values of Z are identified, each corresponding to a distinct functional behavior of the correlation functions between the variables X and Y . Note that our analysis of the function $MIz(m)$ also allows us to distinguish between positive and negative regulatory interactions. These are associated respectively by an increase in MIz for larger values of z_m or decrease of MIz for larger values of z_m . In the Supplementary Figures S1-S2, we display further examples of the function MIz for triadic triples. We observe that as the parameter Γ is raised, the noise increases, which is reflected also in the increased variability of the MIz functional behavior.

In order to provide an overall assessment of the performance of Triaction in mining triadic interactions on this network, in Figure 4(b) we display the Receiver Operating Characteristic curve (ROC curve) based on the score Θ_Σ , which we found to perform well for a wide range of parameters. Our numerical results show a very good performance for larger values of α , and smaller Γ (see Figure 4(b)). As it is apparent from the ROC curve, the Triaction algorithm performs better for higher values of α and smaller values of Γ . For any values of the parameters, we notice that the false positives are more likely involving short-range triples, i.e. triples in which the regulator node Z has short (small) structural network distance with the two nodes X and Y .

V. DETECTING TRIADIC INTERACTIONS IN GENE-EXPRESSION DATA

Searching for trigenic interactions in gene-expression is a problem of major interest in biology. For instance, understanding the extent to which a modulator promotes or silences the interplay between a transcription factor and its target gene is crucial for deciphering gene regulation mechanisms. In order to address this question with our method, we considered gene-expression data from Acute Myeloid Leukemia (AML), extracted from the Grand Gene Regulatory Network Database [39, 40]. This dataset comprises $N = 639$ genes and $R = 151$ samples. Of course, this is for illustration and validation; the same analysis can be made on any gene expression data derived from human tissues, cancer, cell lines, or small molecule drugs as well as on any other dataset arising from different application domains such as climate data, where triadic interactions on networked data are relevant.

Exhaustive mining of all potential triadic interactions among each triple of nodes in the AML dataset is computationally very demanding (it would require testing of $> 260M$ triplets). Instead, we focus on edges associated with known biophysical interactions, as identified in the human Protein-Protein Interaction network (PPI) [39]. To do so, we considered the subgraph of the human PPI network that contains all the genes/proteins included in

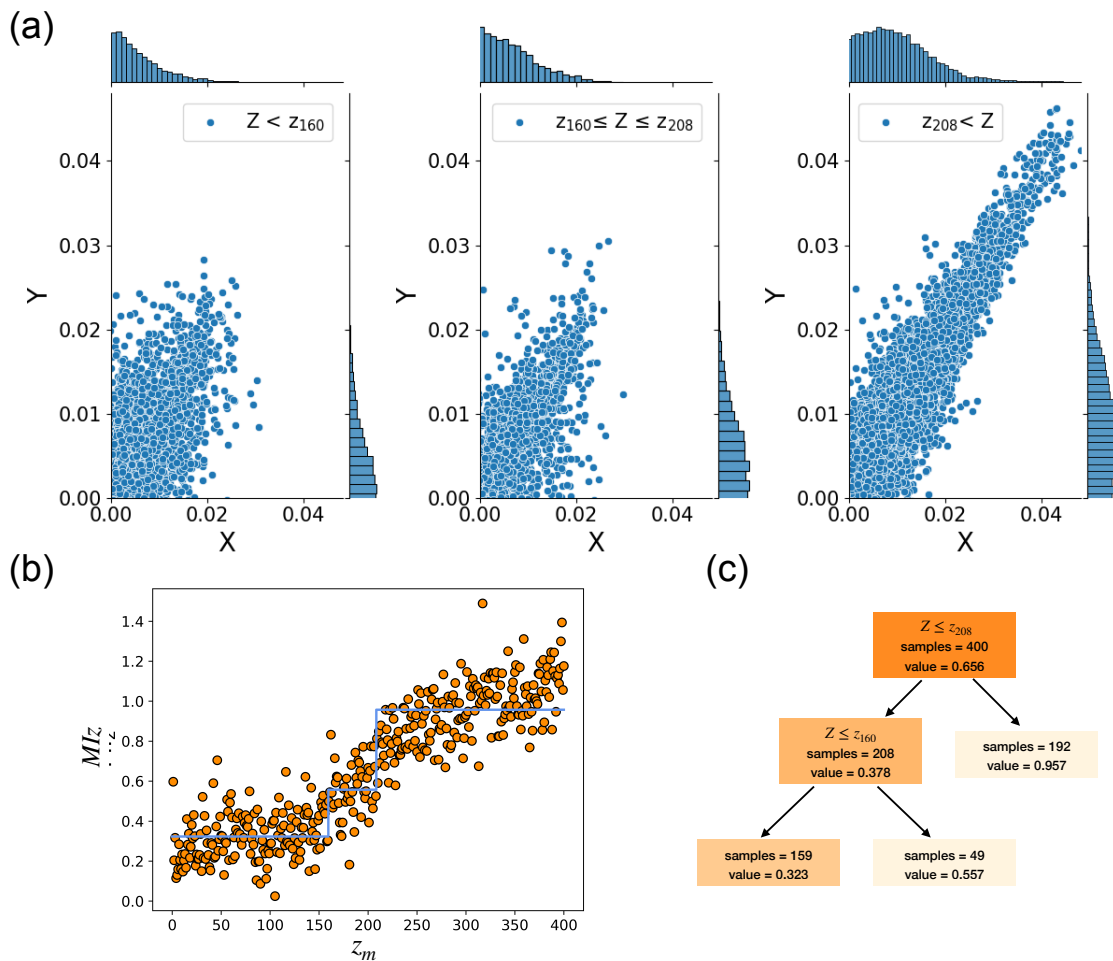


Figure 3. Representative results for a triples of nodes involved in triadic interactions in the continuous model with triadic interactions. The joint distributions of variables X and Y conditional on the values of Z are shown in panel (a). Panel (b) shows the behavior of MIz as a function of the values of z_m , which clearly departs from the constant behavior expected in absence of triadic interactions. Panel (c) presents the decision tree for fitting the MIz functional behavior and determining the range of values of Z for which the most significant differences among the joint distributions of the variables X and Y conditioned on Z are observed. For more details about the simulation result, we refer to the Supplementary Material.

the AML gene expression data. The number of edges in this subgraph is $M = 42,511$. We further refined our choice of candidate triples based on the pairwise information of the PPI network. We considered two random samples of short-range and longer-range triples formed by $\mathcal{P} = 5000$ triples each (see the Supplementary Material for details). Here, range refers to the distance on the structural network between the regulator node Z and the nodes X or Y .

Here we present the results obtained by our mining algorithm using Θ_Σ as the significance score, $P = 5$ bins, and assessed by running $\mathcal{N} = 5 \times 10^3$ realizations of the null model. These results have strong correlations with the results obtained with the other measures (see Supplementary Figures S3-S4 for comparison).

Figure 5(a) displays the results of our algorithm for both for short-range and longer-range triples, involving a structural edge associated the mutual information MI

and the conditional mutual information CMI between its two end-nodes. In the figure, each considered triple corresponds to a point, color coded according to the value of Σ . Low values of Σ correlate with low values of MI and low values of CMI, while the high values of Σ are typically found for data corresponding to higher values of MI and CMI. Figure 5(b) provides data from two exemplar triples: the top panels present evidence of a triadic interaction with high significance score ($\Theta_\Sigma = 3.02$, $p_\Sigma = 0.0024$), while the bottom panels present evidence of a triadic interaction with low significance score ($\Theta_\Sigma = 0.97$, $p_\Sigma = 0.84$). The modulation of the strength of the interactions in the top panels is demonstrated by the significantly different conditional distributions of gene-expression X and Y depending on the value of the gene-expression Z . On the other hand, in the bottom panels the conditional distributions do not change significantly depending on the value of the gene-

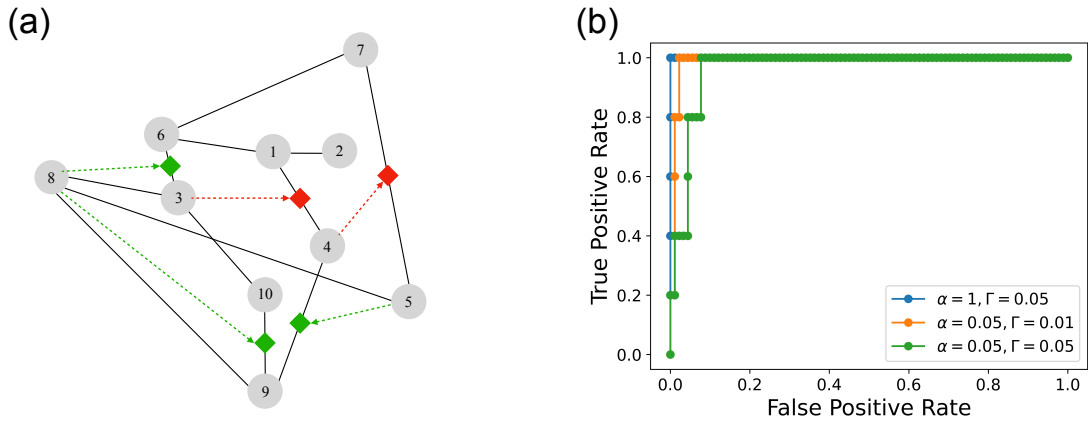


Figure 4. We consider a network with $N = 10$, nodes $L = 12$ edges, and $\hat{L} = 5$ regulatory interactions (panel (a)). The time series obtained by integrating the stochastic dynamics of the proposed dynamical model for triadic interactions (Eq.(7)) are analyzed with the Triaction algorithm. Panel (b) displays the Receiver Operating Characteristic curve (ROC curve) obtained by running Triaction with $P = 400$ bins and $\mathcal{N} = 10^3$ realizations of the null model on these synthetic time series, using Θ_Σ to score for different parameters values indicated in the legend. The time series is simulated up to a maximum time $t_{max} = 4000$ with a $dt = 10^{-2}$. For the analysis, we consider 40000 time steps (see the Supplementary Material for details). The parameters of the model are: $\hat{T} = 10^{-3}$, $w^+ = 8$, $w^- = 0.5$, and α and Γ as indicated in the figure legend.

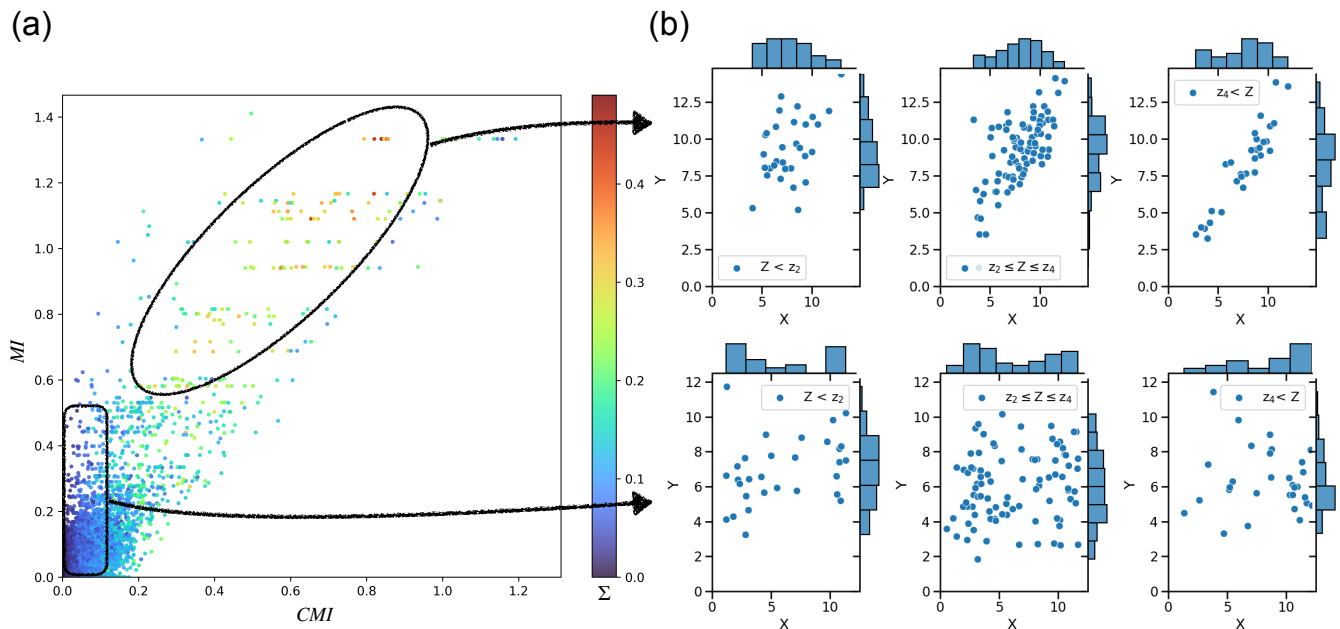


Figure 5. (a) Scatter plot of the results of the Triaction algorithm on AML gene expression data. Each data point shows the information-theoretic measures for a triple of nodes X , Y and Z , namely MI and CMI, the mutual information and conditional mutual information between X and Y , respectively. The colour of each point corresponds to the value of Σ , which characterises the strength of the triadic interaction between gene Z and the edge between X and Y . (b) The results of the decision tree allow us to distinguish three intervals of the value of Z in which the conditional distribution of the gene expression of X and Y differs the most. Plots of these conditional distributions are provided for two exemplary triples: the top one displays a high significance score for the triadic interaction, indicating a meaningful biological association ($X = \text{GATA1}$, $Y = \text{TAL1}$, $Z = \text{KLF5}$, $\Theta_\Sigma = 3.07$, $p_\Sigma = 0.0038$, $\Sigma = 0.27$, $z_2 = 5.3$, $z_4 = 7.2$); the bottom one displays a low significance score ($X = \text{AR}$, $Y = \text{NR4A3}$, $Z = \text{FLI1}$, $\Theta_\Sigma = 0.99$, $p_\Sigma = 0.838$, $\Sigma = 0.024$, $z_2 = 12.9$, $z_4 = 13.3$)

expression Z . For further examples of results obtained on gene-expression triples, see the Supplementary Material.

From this analysis, we can extract a subnetwork (Figure S5(a)) formed by node triplets with a high signifi-

cance score, $p_{\Sigma} < 0.001$ in this case. Blue nodes and edges compose the structural network, that is, the PPI network. Structural edges are represented as black diamonds (factor nodes), while dashed lines illustrate triadic interactions between a regulatory node and a structural edge. We observe that the genes involved in the highest triadic interactions regulation are genes that play a critical role in AML (Figure S5 and Table I): the HOX family [41], PBX3 [42], and MEIS1 [43]. We also investigated the triadic interactions involving a particular edge, such as HOXB5-HOXB6 shown on Table I and Figure S5(b). In particular, most of the top regulatory nodes are consistent across all three measures (Σ, T, T_n).

In the gene-expression literature, previous studies have proposed methods to detect modulation of interactions [16]. Our algorithm goes beyond this previous studies as it allows to detect not only strong monotonous positive and negative triadic interactions (see Supplementary Figure S6 and S7) but also strong triadic interactions with non monotonous MIz functional behavior (see Supplementary Figure S8). The detected interactions strongly depart from triples with low significance score for which the MIz does not vary significantly (see Supplementary Figure S9). Such results challenge the constraints of monotonic assumptions in existing measures within the gene expression literature. It is important to note that, while the monotonic assumption holds in the gene-expression context, non-monotonic behavior is a rare occurrence. However, in broader systems, the prevalence of mostly monotonic behavior, as observed in gene expression, cannot be assumed. Our measures can detect various functional behaviors, and are applicable to any context where triadic interactions may occur.

VI. CONCLUSIONS

Our work proposes a comprehensive information theory approach to model and mine triadic interactions between continuous variables. The key observation is that

the mutual information between two variables can be significantly modulated by a third regulatory node. Hence, detecting triadic interactions requires going beyond pairwise measures such as the mutual information and the conditional mutual information. The proposed approach is here used to mine triadic interactions in gene expression data, and we are able to detect known triadic interactions together with new candidate triplets. Our approach outperforms classical methods in the gene expression community, which assume that the CMI function should exhibit monotonicity with the evolution of the conditioning node [16], and extends the method for broader applications. These results are encouraging and may inspire further research in the field of gene regulation, particularly within the context of tissue specificity. Investigating the extent to which triadic interactions are tissue-specific, as well as whether certain regulatory patterns are conserved across different tissues, could yield valuable insights. In the future, the method could be applied to other type of data including times series which can be relevant in other scientific applications, such as climate research.

CODE AVAILABILITY

The Python package `Triaction` is available on GitHub at the following link: <https://github.com/anthbapt/triaction>

ACKNOWLEDGMENTS

This research utilized Queen Mary’s Apocrita HPC facility, supported by QMUL Research-IT, <https://doi.org/10.5281/zenodo.438045>. A.B., R. S.-G. and G. B. acknowledge support from the Turing-Roche North Star partnership. J. Y. acknowledges financial support from the ITO Foundation for International Education Exchange.

-
- [1] Ginestra Bianconi. *Higher-Order Networks*. Elements in the Structure and Dynamics of Complex Networks. Cambridge University Press, Cambridge, 2021.
 - [2] Federico Battiston, Enrico Amico, Alain Barrat, Ginestra Bianconi, Guilherme Ferraz de Arruda, Benedetta Franceschiello, Iacopo Iacopini, Sonia Kéfi, Vito Latora, Yamir Moreno, Micah M. Murray, Tiago P. Peixoto, Francesco Vaccarino, and Giovanni Petri. The physics of higher-order interactions in complex systems. *Nature Physics*, 17(10):1093–1098, 2021.
 - [3] Federico Battiston, Giulia Cencetti, Iacopo Iacopini, Vito Latora, Maxime Lucas, Alice Patania, Jean-Gabriel Young, and Giovanni Petri. Networks beyond pairwise interactions: structure and dynamics. *Physics Reports*, 874:1–92, 2020.
 - [4] Leo Torres, Ann S Blevins, Danielle Bassett, and Tina Eliassi-Rad. The why, how, and when of representations for complex systems. *SIAM Review*, 63(3):435–485, 2021.
 - [5] Christian Bick, Elizabeth Gross, Heather A. Harrington, and Michael T. Schaub. What are higher-order networks?, 2022.
 - [6] Guido Previde Massara, Tiziana Di Matteo, and Tomaso Aste. Network filtering for big data: Triangulated maximally filtered graph. *Journal of complex Networks*, 5(2):161–178, 2016.
 - [7] Jean-Gabriel Young, Giovanni Petri, and Tiago P. Peixoto. Hypergraph reconstruction from network data. *Communications Physics*, 4(1):135, 2021.

Regulator	node1	node2	rank Σ	Θ_Σ	P_Σ	rank T	Θ_T	P_T	rank T_n	Θ_{T_n}	P_{T_n}
MEIS1	HOXB5	HOXB6	1	6.94	0.0002	1	6.64	0.0002	1	6.66	0.0002
ETS2	HOXB5	HOXB6	2	5.32	0.0002	2	5.93	0.0002	17	3.41	0.0028
HOXA3	HOXB5	HOXB6	3	5.23	0.0002	3	5.81	0.0002	27	2.75	0.0096
UNCX	HOXB5	HOXB6	4	5.01	0.0002	5	4.86	0.0002	7	4.46	0.0002
THRA	HOXB5	HOXB6	5	4.92	0.0002	4	5.45	0.0002	2	6.02	0.0002
HOXB7	HOXB5	HOXB6	11	4.14	0.0004	6	4.27	0.0006	4	4.86	0.0002
FOSL1	HOXB5	HOXB6	12	4.06	0.0002	8	4.23	0.0002	3	4.90	0.0002
HOXB8	HOXB5	HOXB6	14	3.93	0.0002	7	4.26	0.0002	5	4.82	0.0002

Table I. The list of the top 5 high-significant triples for the three measures Σ, T, T_n involving the structural network edge HOXB5-HOXB6. Across all three measures (Σ, T , and T_n), the top triadic interaction involves MEIS1 as the regulatory node. The second highest regulatory node for the HOXB5-HOXB6 edge is ETS2 for the Σ and T measures, and THRA for the T_n measure. Notably, THRA also ranks highly for the Σ measure (ranked 5) and the T measure (ranked 4). The third highest regulatory node for the HOXB5-HOXB6 edge is HOXA3 for both the Σ and T measures, and FOSL1 for the T_n measure.

- [8] Martina Contisciani, Federico Battiston, and Caterina De Bacco. Inference of hyperedges and overlapping communities in hypergraphs. *Nature Communications*, 13(1):7229, 2022.
- [9] Federico Musciotto, Federico Battiston, and Rosario N Mantegna. Detecting informative higher-order interactions in statistically validated hypergraphs. *Communications Physics*, 4(1):218, 2021.
- [10] Robin Delabays, Giulia De Pasquale, Florian Dörfler, and Yuanzhao Zhang. Hypergraph reconstruction from dynamics. *arXiv preprint arXiv:2402.00078*, 2024.
- [11] Eckehard Olbrich, Nils Bertschinger, and Johannes Rauh. Information decomposition and synergy. *Entropy*, 17(5):3501–3517, 2015.
- [12] Fernando E Rosas, Pedro AM Mediano, Michael Gastpar, and Henrik J Jensen. Quantifying high-order interdependencies via multivariate extensions of the mutual information. *Physical Review E*, 100(3):032305, 2019.
- [13] Sebastiano Stramaglia, Tomaso Scagliarini, Bryan C Daniels, and Daniele Marinazzo. Quantifying dynamical high-order interdependencies from the o-information: An application to neural spiking dynamics. *Frontiers in Physiology*, 11:595736, 2021.
- [14] Michele Tumminello, Tomaso Aste, Tiziana Di Matteo, and Rosario N Mantegna. A tool for filtering information in complex systems. *Proceedings of the National Academy of Sciences*, 102(30):10421–10426, 2005.
- [15] Juan Zhao, Yiwei Zhou, Xiujun Zhang, and Luonan Chen. Part mutual information for quantifying direct associations in networks. *Proceedings of the National Academy of Sciences*, 113(18):5130–5135, May 2016.
- [16] Kai Wang, Masumichi Saito, Brygida C. Bisikirska, Mariano J. Alvarez, Wei Keat Lim, Presha Rajbhandari, Qiong Shen, Ilya Nemenman, Katia Basso, Adam A. Margolin, Ulf Klein, Riccardo Dalla-Favera, and Andrea Califano. Genome-wide identification of post-translational modulators of transcription factor activity in human b cells. *Nature Biotechnology*, 27(9):829–837, 2009.
- [17] Dror Y. Kenett, Xuqing Huang, Irena Vodenska, Shlomo Havlin, and H. Eugene Stanley. Partial correlation analysis: applications for financial markets. *Quantitative Finance*, 15(4):569–578, April 2015.
- [18] Hanlin Sun, Filippo Radicchi, Jürgen Kurths, and Ginestra Bianconi. The dynamic nature of percolation on networks with triadic interactions. *Nature Communications*, 14(1):1308, 2023.
- [19] Eyal Bairey, Eric D. Kelsic, and Roy Kishony. High-order species interactions shape ecosystem diversity. *Nature Communications*, 7(1):12285, 2016.
- [20] Jacopo Grilli, György Barabás, Matthew J. Michalska-Smith, and Stefano Allesina. Higher-order interactions stabilize dynamics in competitive network models. *Nature*, 548(7666):210–213, 2017.
- [21] Andrew D. Letten and Daniel B. Stouffer. The mechanistic basis for higher-order interactions and non-additivity in competitive communities. *Ecol Lett*, 22(3):423–436, March 2019.
- [22] Woo-Hyun Cho, Ellane Barcelon, and Sung Joong Lee. Optogenetic glia manipulation: Possibilities and future prospects. *Experimental Neurobiology*, 25(5):197–204, October 2016.
- [23] Federico M. Giorgi, Gonzalo Lopez, Jung H. Woo, Brygida Bisikirska, Andrea Califano, and Mukesh Bansal. Inferring protein modulation from gene expression data using conditional mutual information. *PLOS ONE*, 9(10):e109569, October 2014.
- [24] Ana P Millán, Hanlin Sun, Joaquín J Torres, and Ginestra Bianconi. Triadic percolation induces dynamical topological patterns in higher-order networks. *arXiv preprint arXiv:2311.14877*, 2023.
- [25] Lukas Herron, Pablo Sartori, and BingKan Xue. Robust retrieval of dynamic sequences through interaction modulation. *PRX Life*, 1(2):023012, 2023.
- [26] Leo Kozachkov, Jean-Jacques Slotine, and Dmitry Krotov. Neuron-astrocyte associative memory. *arXiv preprint arXiv:2311.08135*, 2023.
- [27] Giorgio Nicoletti and Daniel Maria Busiello. Information propagation in multilayer systems with higher-order interactions across timescales. *Physical Review X*, 14(2):021007, 2024.
- [28] Elena Kuzmin, Benjamin VanderSluis, Wen Wang, Guihong Tan, Raamesh Deshpande, Yiqun Chen, Matej Usaj, Attila Balint, Mojca Mattiazzi Usaj, Jolanda van Leeuwen, Elizabeth N. Koch, Carles Pons, Andrius J. Dagilis, Michael Pryszlak, Jason Zi Yang Wang, Julia Hanchard, Margot Rigg, Kaicong Xu, Hamed Heydari, Bryan-Joseph San Luis, Ermira Shuteriqi, Hongwei Zhu, Nydia Van Dyk, Sara Sharifpoor, Michael Costanzo, Robbie Loewith, Amy Caudy, Daniel Bolnick, Grant W. Brown, Brenda J. Andrews, Charles Boone, and Chad L. Myers. Systematic analysis of complex genetic interac-

- tions. *Science*, 360(6386):eaao1729, April 2018.
- [29] Leonie Neuhäuser, Renaud Lambiotte, and Michael T Schaub. Consensus dynamics and opinion formation on hypergraphs. In *Higher-Order Systems*, pages 347–376. Springer, 2022.
- [30] Leonie Neuhäuser, Andrew Mellor, and Renaud Lambiotte. Multibody interactions and nonlinear consensus dynamics on networked systems. *Physical Review E*, 101(3):032310, 2020.
- [31] Iacopo Iacopini, Giovanni Petri, Alain Barrat, and Vito Latora. Simplicial models of social contagion. *Nature communications*, 10(1):2485, 2019.
- [32] Guilherme Ferraz de Arruda, Giovanni Petri, and Yamir Moreno. Social contagion models on hypergraphs. *Physical Review Research*, 2(2):023032, 2020.
- [33] Petar Veličković, Guillem Cucurull, Arantxa Casanova, Adriana Romero, Pietro Lio, and Yoshua Bengio. Graph attention networks. *arXiv preprint arXiv:1710.10903*, 2017.
- [34] Lyudmyla F Kozachenko and Nikolai N Leonenko. Sample estimate of the entropy of a random vector. *Problemy Peredachi Informatsii*, 23(2):9–16, 1987.
- [35] Alexander Kraskov, Harald Stögbauer, and Peter Grassberger. Estimating mutual information. *Physical review E*, 69(6):066138, 2004.
- [36] Brian C Ross. Mutual information between discrete and continuous data sets. *PloS one*, 9(2):e87357, 2014.
- [37] J Kurths and H Herzel. An attractor in a solar time series. *Physica D: Nonlinear Phenomena*, 25(1-3):165–172, 1987.
- [38] James Theiler, Stephen Eubank, André Longtin, Bryan Galdrikian, and J Doyné Farmer. Testing for nonlinearity in time series: the method of surrogate data. *Physica D: Nonlinear Phenomena*, 58(1-4):77–94, 1992.
- [39] Marouen Ben Guebila, Camila M Lopes-Ramos, Deborah Weighill, Abhijeet Rajendra Sonawane, Rebekka Burkholz, Behrouz Shamsaei, John Platig, Kimberly Glass, Marieke L Kuijjer, and John Quackenbush. "grand gene regulatory network database", 2023.
- [40] Marouen Ben Guebila, Camila M. Lopes-Ramos, Deborah Weighill, Abhijeet Rajendra Sonawane, Rebekka Burkholz, Behrouz Shamsaei, John Platig, Kimberly Glass, Marieke L. Kuijjer, and John Quackenbush. Grand: a database of gene regulatory network models across human conditions. *Nucleic Acids Res*, 50(D1):D610–D621, January 2022.
- [41] R. A. Alharbi, R. Pettengell, H. S. Pandha, and R. Morgan. The role of hox genes in normal hematopoiesis and acute leukemia. *Leukemia*, 27(5):1000–1008, 2013.
- [42] Huidong Guo, Yajing Chu, Le Wang, Xing Chen, Yang-peng Chen, Hui Cheng, Lei Zhang, Yuan Zhou, Feng-chun Yang, Tao Cheng, Mingjiang Xu, Xiaobing Zhang, Jianfeng Zhou, and Weiping Yuan. Pbx3 is essential for leukemia stem cell maintenance in mll-rearranged leukemia. *Int. J. Cancer*, 141(2):324–335, July 2017.
- [43] Ping Xiang, Xining Yang, Leo Escano, Ishpreet Dhillon, Edith Schneider, Jack Clemans-Gibbon, Wei Wei, Jasper Wong, Simon Xufeng Wang, Derek Tam, Yu Deng, Eric Yung, Gregg B. Morin, Pamela A. Hoodless, Martin Hirst, Aly Karsan, Florian Kuchenbauer, R. Keith Humphries, and Arefeh Rouhi. Elucidating the importance and regulation of key enhancers for human meis1 expression. *Leukemia*, 36(8):1980–1989, 2022.

Supplemental Material on “Mining higher-order triadic interactions”

Anthony Baptista,^{1,2} Marta Niedostatek,¹ Jun Yamamoto,³ Ben MacArthur,^{2,4,5}
Jürgen Kurths,^{6,7} Ruben Sanchez Garcia,^{2,4} and Ginestra Bianconi^{1,2}

¹*School of Mathematical Sciences, Queen Mary University of London, London, E1 4NS, United Kingdom*

²*The Alan Turing Institute, The British Library, London, NW1 2DB, United Kingdom*

³*Department of Network and Data Science, Central European University, Vienna 1100, Austria*

⁴*School of Mathematical Sciences, University of Southampton, Southampton SO17 1BJ, United Kingdom*

⁵*Faculty of Medicine, University of Southampton, Southampton SO17 1BJ, United Kingdom*

⁶*Potsdam Institute for Climate Impact Research, 14473 Potsdam, Germany*

⁷*Institute of Physics, Humboldt University of Berlin, 12489 Berlin, Germany*

SUPPLEMENTAL INFORMATION ON THE TRIADIC MODEL WITHIN CONTINUOUS VARIABLES.

We use a network with $N = 10$ nodes $L = 12$ edges and $\hat{L} = 5$ regulatory interactions (shown in Figure 3 of the main text). We consider the time series obtained by integrating the stochastic dynamics of the proposed dynamical model for triadic interactions within continuous variables. The time series is simulated up to a maximum time $t_{max} = 4000$ with a $dt = 10^{-2}$ leading to 4×10^5 data points. For our analysis we consider the last 200,000 data points sampled every fifth point leading to 40,000 time steps. In Figure 2 of the main text we report the analysis done for the triplet [4,9,5], which is triadic. For this figure the parameters of the model are: $\alpha = 0.05, \hat{T} = 10^{-3}, \Gamma = 10^{-2}, w^+ = 8, w^- = 0.5$, number of bins $P = 400$. In the Supplemental Figures S1 and S2 we report the analysis conducted on the same triadic triple of nodes for different parameter values: for Figure S1 we have $\alpha = 0.01, \Gamma = 10^{-2}$, for Figure S2 we have $\alpha = 0.05, \Gamma = 5 \times 10^{-2}$. The other parameter values are the same as in Figure 2 of the main text.

SUPPLEMENTAL INFORMATION ON ANALYSIS OF GENE-EXPRESSION DATASET

Triplet selection

We choose two sub-samples of 5000 triples of triadic interactions from the gene-expression associated with Acute Myeloid Leukemia (AML) dataset for our Triaction analyses. The selection process for these sub-samples is motivated by studies indicating that for gene expression data, most of the genes involved in trigenic processes are also involved in digenic processes [1]. Hence, we utilize the Protein-Protein Interaction network (PPI) associated with AML, which captures digenic processes, to choose edges forming the triplets in our study. The selection of the regulatory node aims to encompass both short-range and longer-range interactions. To differentiate between these cases, we employ the shortest path distance in the PPI. The first sub-sample comprises short-range motifs, including the fully connected triangle and the partially connected triangle (see Figure S3(a)). We conduct a similar analysis for longer-range interactions. Figure S3(a) illustrates the distribution of the proportion of triplets categorized by the length of the shortest path between node Z and the edge composed of nodes X and Y. This path length can be expressed as $\min(d_{XZ}, d_{YZ})$, where d_{XZ} denotes the shortest path length between nodes X and Z, and d_{YZ} indicates the shortest path length between nodes Y and Z.

Comparison between short-range and longer range triples in AML dataset

Based on the structural network, specifically the Protein-Protein Interaction network (PPI), we distinguish interactions into short-range (depicted in blue) and longer-range (depicted in red). Longer-range interactions are characterised by a minimum shortest path between structural edges and the regulatory node candidate of at least 2. S3(b) display the probability density function estimated by Gaussian kernels on the histogram of the probability distribution of the score Θ for the three measures: Σ , T , and T_n . Curves in varying shades of blue represent short-range interactions, while those in shades of red represent longer-range interactions. Notably, significant Θ scores are predominantly associated with short-range interactions. S3(e-f) showcase correlations between Θ scores for the three measures. There is a strong correlation between Θ_Σ and Θ_T (S3(e)), these correlation is observed both for short- and long-range interactions. The correlation is also observed between Θ_Σ and Θ_{T_n} (S3(f)). S3(c-d) display mutual information between nodes (X and Y) involved in structural edges, as well as mutual information between X and

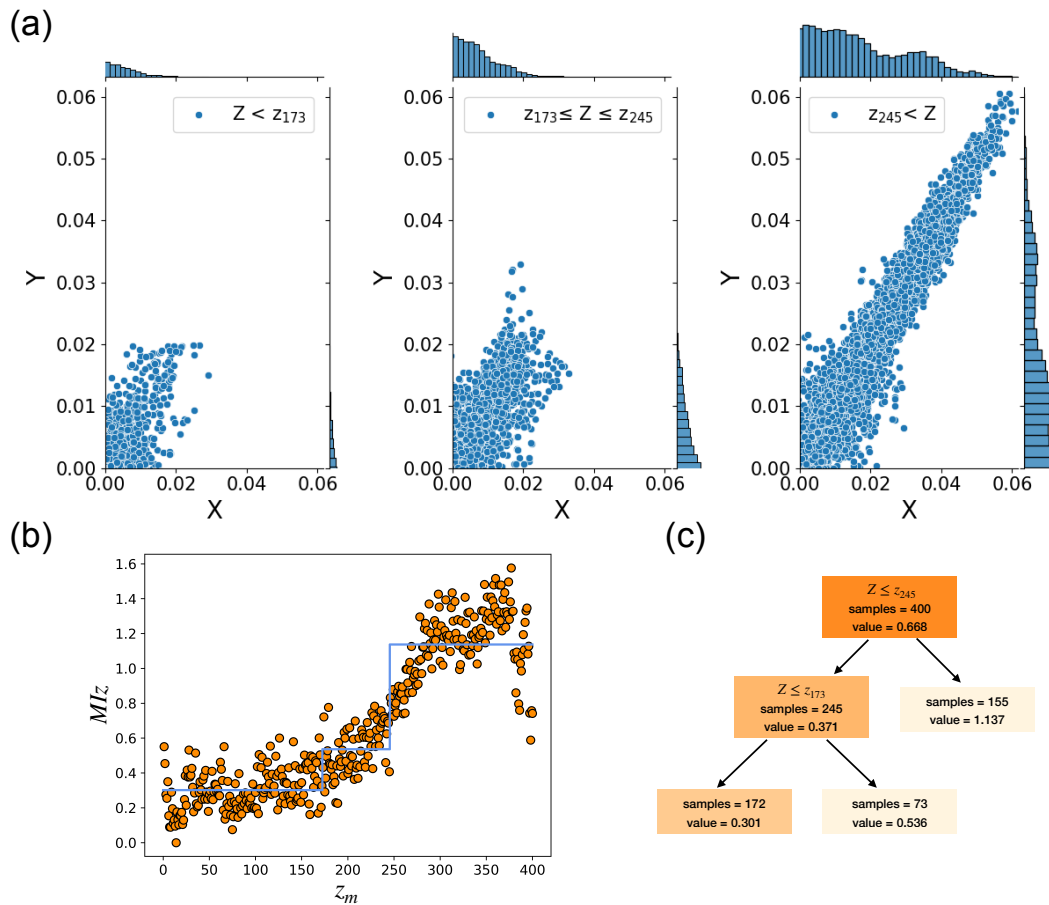


FIG. S1: Exemplary results obtained for a triple of nodes involved in a triadic interactions in the continuous model with triadic interactions. The joint distributions of variables X and Y conditional on the values of Z is shown in panel (a). Panel (b) displays the functional behavior of MIz as a function of the values of z_m which clearly departs from the constant behavior expected in absence of triadic interactions. Panel (c) presents the decision tree for fitting the MIz functional behavior and determining the range of values of Z for which the most significant differences among the joint distributions of the variables X and Y conditional to Z are observed. For more details about the simulation result we refer to the Supplemental Material. The time series is simulated up to a maximum time $t_{max} = 4000$ with a $dt = 10^{-2}$. For the analysis we consider 40000 time steps. The parameters of the model are: $\alpha = 0.01$, $\hat{T} = 10^{-3}$, $\Gamma = 10^{-2}$, $w^+ = 8$, $w^- = 0.5$, number of bins $P = 400$. The analysis is done for the triplet $[4,9,5]$, of the network in Figure 2 of the main text, which is triadic.

Y conditioned by the third node (Z), which is designated as the regulatory node. Colour denotes the logarithm of the inverse of the P-value of the Σ measure (P_Σ), emphasising significant P-values. Red dots represent short-range interactions (S3(c)), while blue dots represent longer-range interactions (S3(d)). Observations indicate that significant triplets, particularly for short-range interactions, necessitate high mutual information and conditional mutual information. However, for longer-range interactions, conditional mutual information must be higher than mutual information.

Comparison between the results obtained with different measures

In Figure S4 we display the results obtained on the gene-expression AML data by performing an analysis conducted using the T and the T_n measures. We observe that these results correlate with the results obtained using the Σ measure reported in Fig.4 of the main text.

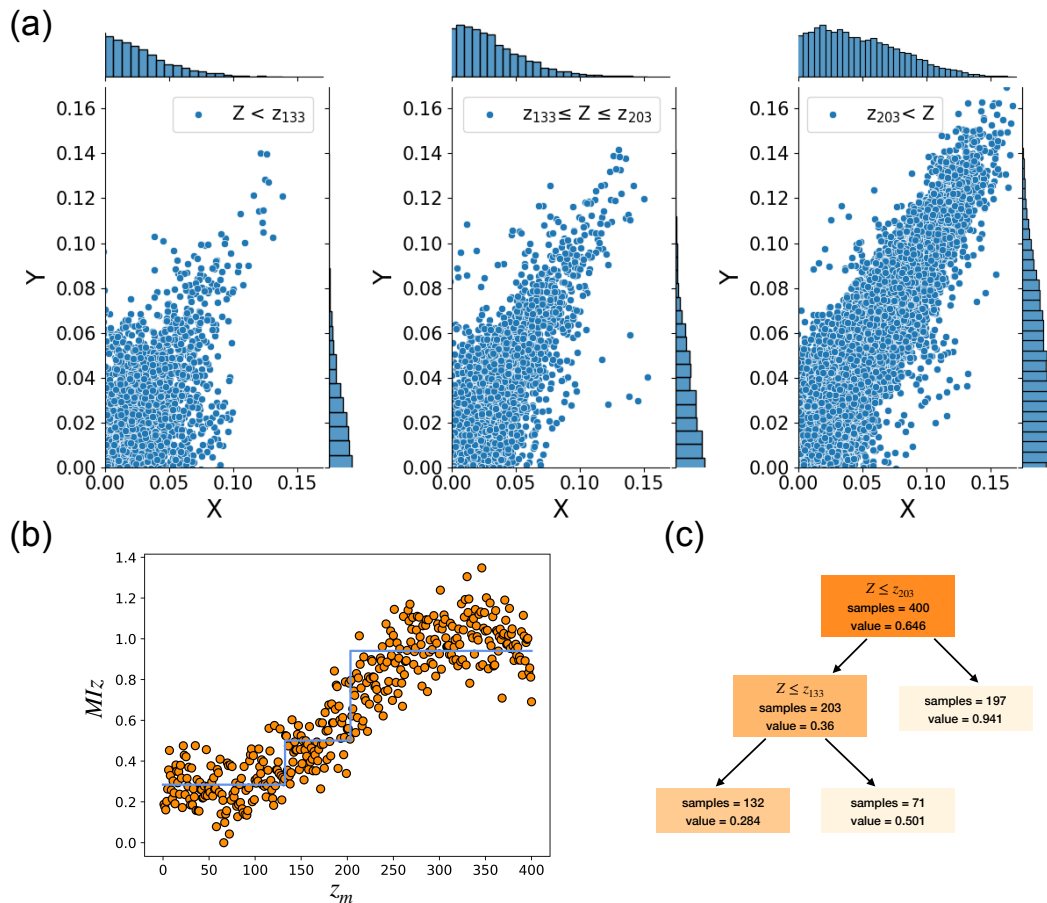


FIG. S2: Exemplary results obtained for a triplet of nodes involved in a triadic interactions in the continuous model with triadic interactions. The joint distributions of variables X and Y conditional on the values of Z is shown in panel (a). Panel (b) displays the functional behavior of MIz as a function of the values of z_m which clearly departs from the constant behavior expected in absence of triadic interactions. Panel (c) presents the decision tree for fitting the MIz functional behavior and determining the range of values of Z for which the most significant differences among the joint distributions of the variables X and Y conditional to Z are observed. For more details about the simulation result we refer to the Supplemental Material. The time series is simulated up to a maximum time $t_{max} = 4000$ with a $dt = 10^{-2}$. For the analysis we consider 40000 time steps (see SM for details). The parameters of the model are: $\alpha = 0.05$, $\hat{T} = 10^{-3}$, $\Gamma = 5 \times 10^{-2}$, $w^+ = 8$, $w^- = 0.5$, number of bins $P = 400$. The analysis is done for the triplet $[4,9,5]$, of the network in Figure 2 of the main text, which is triadic.

Supplemental figure and table of detected triadic interactions in AML dataset

We detected 32 triadic interactions with a $p_\Sigma < 0.001$, listed in Table S1. In the Table, we report Σ, T, T_n , $\Theta_\Sigma, \Theta_T, \Theta_{T_n}$ and the p-values p_Σ, p_T, p_{T_n} associated with each triadic interaction of the network displayed in Figure S5. We observe that the genes involved in the highest triadic interactions regulation are genes to play a critical role in AML (Figure 6), the HOX family [2], PBX3 [3], and MEIS1 [4]. Moreover, a recent study shows that HOXA5 is a regulation hub for AML patients [5] which can also be observed in Figure 6. Furthermore, known triple have been detected with a lower p-value threshold like (HOXA9, PBX3, MEIS1, $p_\Sigma = 0.06$) which are known to cooperate all together in AML patients [6, 7].

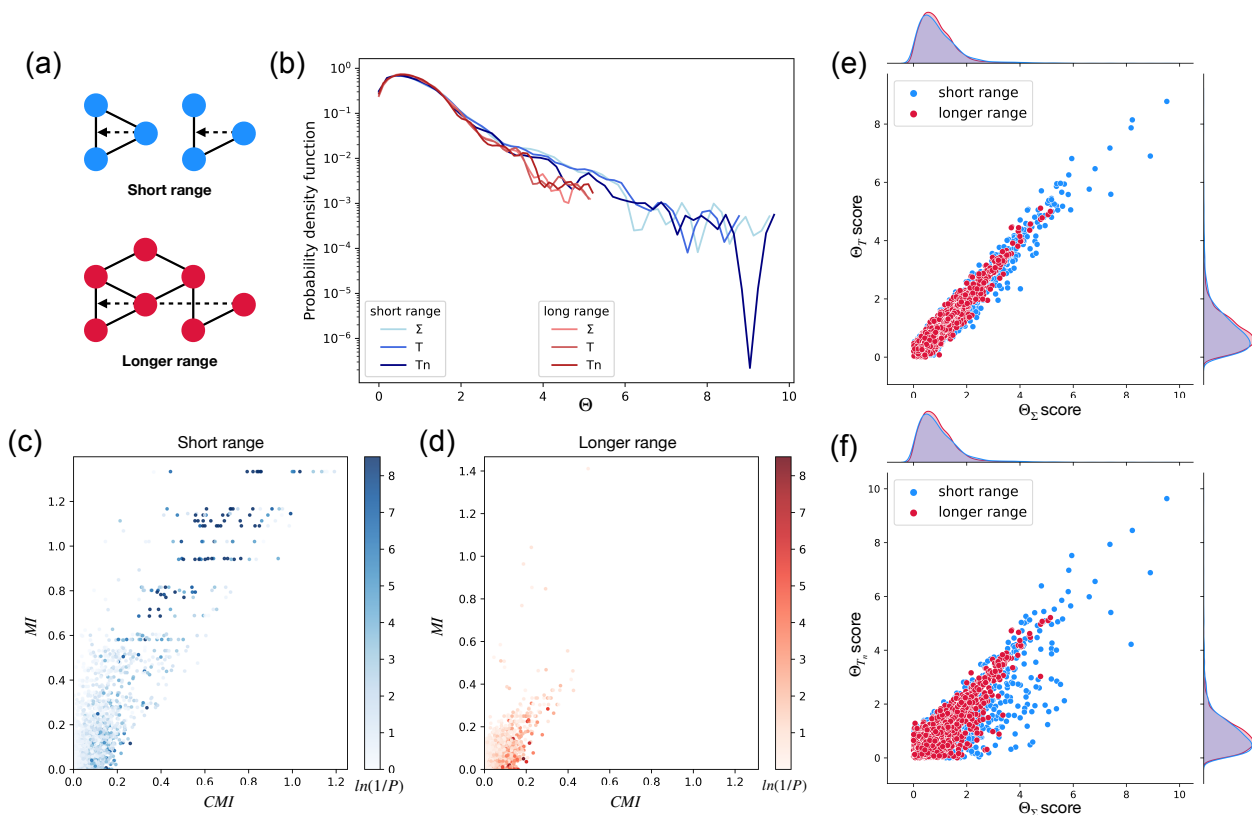


FIG. S3: (a) Candidate triadic interactions occur both at short-range (depicted in blue) and at longer-range (depicted in red). (b) Probability density function of Θ for the three measures: Σ , T , and T_n . Curves in varying shades of blue represent short-range interactions, while those in shades of red represent longer-range interactions. (c-d) Scatter plots of the mutual information between nodes (X and Y) involved in structural edges and the mutual information between X and Y conditioned by the third node (Z). Color denotes the logarithm of the inverse of the P -value of the Σ measure (P_Σ). Red dots represent short-range interactions (c), and blue dots represent longer-range interactions (d). (e-f) Scatter plots between Θ scores for the three measures: between Θ_Σ and Θ_T (e), and Θ_Σ and Θ_{T_n} (f).

Supplemental Figures on gene-expression results

In Figure S6-S9 we display exemplary results obtained by applying the Triaction algorithm on the AML dataset. Figure S6 provides an example of high-significant positive triadic interaction. Figure S6 provides an example of high-significant negative triadic interactions. Figure S8 provides an example of triadic interactions displaying a non-monotonous MI_z functional behavior. Figure S9 provides an example of triple with low significance score for triadic interactions with a almost flat MI_z profile.

TRIACTION PYTHON PACKAGE

The Triaction algorithm here proposed is implemented by a Python package, called Triaction, that we have developed for detecting triadic interactions within continuous and discrete variables. The Triaction package allows to work with both data-frames and data sets associated with a pairwise network. From this initial data, the package provides various ways to extract relevant features and detect triadic interactions. We have included several representations and visualisations in the package to aid in the interpretation of the results. The code is available on GitHub at the following link: <https://github.com/anthbapt/triaction>. Additionally, we offer documentation to guide users through the analysis process.

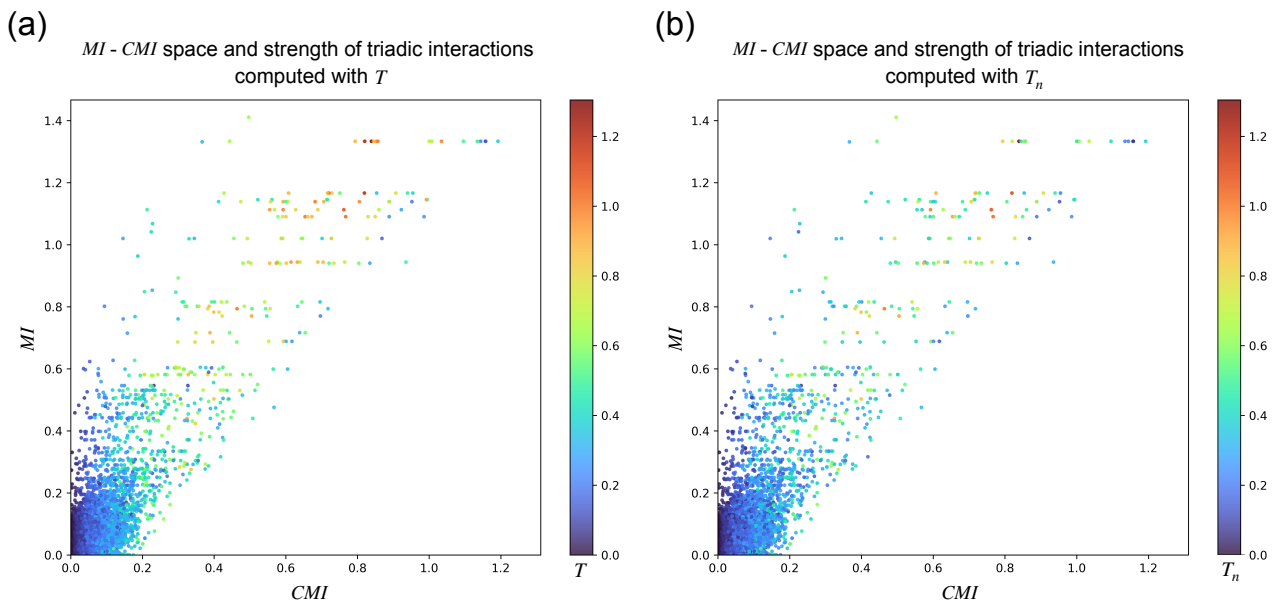


FIG. S4: (a) Scatter plot which displays the MI (Y-axis) value between two genes, denoted X and Y , and the CMI (X-axis) between the same genes X and Y conditioned by a third gene, denoted Z . The colour corresponds to the value of our measure T which characterises the strength of the triadic interaction between gene Z and edge involving X and Y . (b) Same figure for the measure T_n .

-
- [1] Elena Kuzmin, Benjamin VanderSluis, Wen Wang, Guihong Tan, Raamesh Deshpande, Yiqun Chen, Matej Usaj, Attila Balint, Mojca Mattiazzi Usaj, Jolanda van Leeuwen, Elizabeth N. Koch, Carles Pons, Andrius J. Dagilis, Michael Prysizlak, Jason Zi Yang Wang, Julia Hanchard, Margot Riggi, Kaicong Xu, Hamed Heydari, Bryan-Joseph San Luis, Ermira Shuteriqi, Hongwei Zhu, Nydia Van Dyk, Sara Sharifpoor, Michael Costanzo, Robbie Loewith, Amy Caudy, Daniel Bolnick, Grant W. Brown, Brenda J. Andrews, Charles Boone, and Chad L. Myers. Systematic analysis of complex genetic interactions. *Science*, 360(6386):eaao1729, April 2018.
 - [2] R. A. Alharbi, R. Pettengell, H. S. Pandha, and R. Morgan. The role of hox genes in normal hematopoiesis and acute leukemia. *Leukemia*, 27(5):1000–1008, 2013.
 - [3] Huidong Guo, Yajing Chu, Le Wang, Xing Chen, Yangpeng Chen, Hui Cheng, Lei Zhang, Yuan Zhou, Feng-chun Yang, Tao Cheng, Mingjiang Xu, Xiaobing Zhang, Jianfeng Zhou, and Weiping Yuan. Pbx3 is essential for leukemia stem cell maintenance in mll-rearranged leukemia. *Int. J. Cancer*, 141(2):324–335, July 2017.
 - [4] Ping Xiang, Xining Yang, Leo Escano, Ishpreet Dhillon, Edith Schneider, Jack Clemans-Gibbon, Wei Wei, Jasper Wong, Simon Xufeng Wang, Derek Tam, Yu Deng, Eric Yung, Gregg B. Morin, Pamela A. Hoodless, Martin Hirst, Aly Karsan, Florian Kuchenbauer, R. Keith Humphries, and Arefeh Rouhi. Elucidating the importance and regulation of key enhancers for human meis1 expression. *Leukemia*, 36(8):1980–1989, 2022.
 - [5] Huili Wang, Sheng-Yan Lin, Fei-Fei Hu, An-Yuan Guo, and Hui Hu. The expression and regulation of hox genes and membrane proteins among different cytogenetic groups of acute myeloid leukemia. *Molecular genetics & genomic medicine*, 8:e1365, Sep 2020.
 - [6] Ross M. W. Thorne and Thomas A. Milne. Dangerous liaisons: cooperation between pbx3, meis1 and hoxa9 in leukemia. *haematol*, 100(7):850–853, July 2015.
 - [7] Zejuan Li, Ping Chen, Rui Su, Chao Hu, Yuanyuan Li, Abdel G. Elkahlon, Zhixiang Zuo, Sandeep Gurbuxani, Stephen Aronovitz, Hengyou Weng, Yungui Wang, Shenglai Li, Hao Huang, Mary Beth Neilly, Gang Greg Wang, Xi Jiang, Paul P. Liu, Jie Jin, and Jianjun Chen. PBX3 and MEIS1 Cooperate in Hematopoietic Cells to Drive Acute Myeloid Leukemias Characterized by a Core Transcriptome of the MLL-Rearranged Disease. *Cancer Research*, 76(3):619–629, 01 2016.

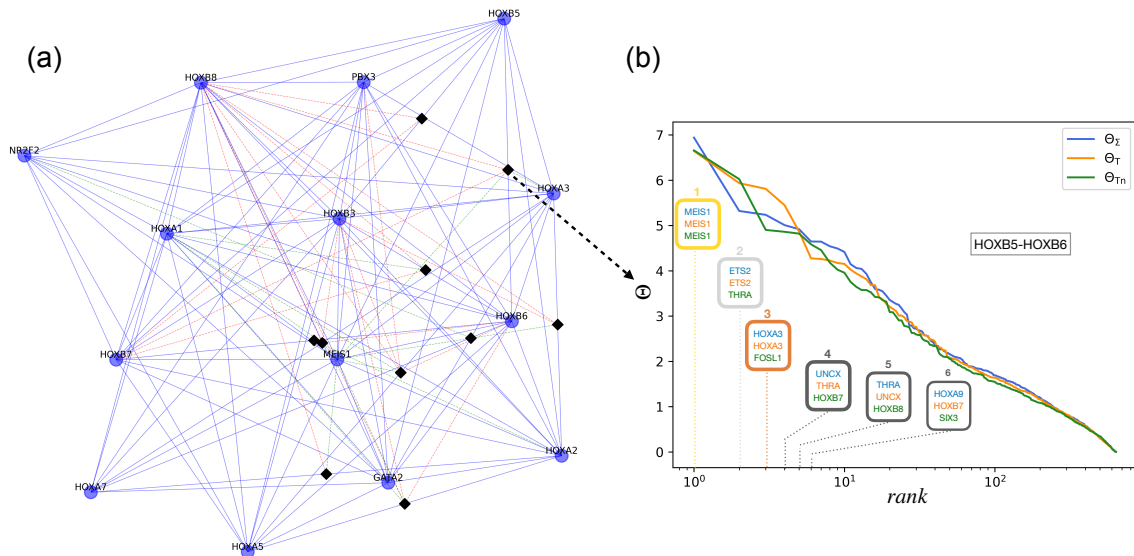


FIG. S5: (a) Visualization of the AML network with triadic interactions mined by the Triaction algorithm including the 32 detected triadic interactions with $p_\Sigma < 10^{-3}$ (see Supplementary Table for the list of such interactions). Blue nodes and edges compose the structural network, which is a subgraph of the Protein-Protein Interaction network (PPI). Factor nodes are depicted as black diamonds, while dashed lines (green for positive and red for negative) illustrate regulatory triadic interactions. (b) We consider all the putative triadic interactions involving the structural network edge HOXB5-HOXB6 and any possible regulatory node. The obtained values of Θ_Σ , Θ_T , and Θ_{Tn} , are plotted against their rank. The nodes associated with the six highest ranked Θ scores are indicated in the insets. Across all three measures (Σ , T , and Tn), the top triadic interaction involves MEIS1 as the regulatory node (depicted in a golden frame inset). The second highest regulatory node for the HOXB5-HOXB6 edge is ETS2 for the Σ and T measures, and THRA for the Tn measure (illustrated in a silver frame inset). Notably, THRA also ranks highly for the Σ measure (ranked 5) and the T measure (ranked 4). The third highest regulatory node for the HOXB5-HOXB6 edge is HOXA3 for both the Σ and T measures, and FOXL1 for the Tn measure (highlighted in a bronze frame-inset).

Regulator	node1	node2	Σ	T	T_n	Θ_Σ	Θ_T	Θ_{T_n}	P_Σ	P_T	P_{T_n}
HOXB3	HOXA2	HOXA5	0.280	0.870	0.518	4.310	5.070	2.437	0.0002	0.0002	0.0164
MEIS1	HOXA3	HOXA5	0.490	1.304	1.304	9.521	8.777	9.634	0.0002	0.0002	0.0002
MEIS1	HOXB5	HOXB6	0.427	1.163	1.082	6.824	6.466	6.555	0.0002	0.0002	0.0002
HOXB6	HOXA2	HOXA5	0.292	0.835	0.530	4.727	4.861	2.598	0.0002	0.0002	0.0130
HOXB8	HOXA2	HOXA5	0.256	0.744	0.571	3.782	4.019	3.005	0.0002	0.0002	0.0050
HOXB3	HOXA2	HOXA3	0.325	0.942	0.715	5.186	5.446	4.059	0.0002	0.0002	0.0002
PBX3	HOXA3	HOXA5	0.438	1.196	0.722	8.179	7.870	4.219	0.0002	0.0002	0.0002
HOXB6	HOXA3	HOXA5	0.326	0.896	0.458	5.372	5.194	1.825	0.0002	0.0002	0.0460
HOXB8	HOXA3	HOXA5	0.329	0.981	0.694	5.372	5.862	4.003	0.0002	0.0002	0.0004
HOXB6	HOXA3	HOXA7	0.262	0.737	0.404	4.447	4.468	1.716	0.0002	0.0002	0.0570
HOXB3	HOXA3	HOXA5	0.330	0.883	0.819	5.421	5.047	5.057	0.0002	0.0002	0.0002
HOXB3	HOXA3	HOXA7	0.291	0.820	0.528	5.180	5.232	2.931	0.0002	0.0002	0.0074
HOXB7	HOXB5	HOXB6	0.309	0.884	0.884	4.258	4.404	5.059	0.0002	0.0002	0.0002
HOXB8	HOXA3	HOXA7	0.371	1.024	1.024	7.383	7.176	7.934	0.0002	0.0002	0.0002
HOXA1	HOXA3	HOXA5	0.411	0.948	0.854	7.416	5.589	5.402	0.0002	0.0002	0.0002
MEIS1	HOXA3	HOXA7	0.428	1.000	0.927	8.901	6.901	6.880	0.0002	0.0002	0.0002
HOXA2	HOXB6	HOXB7	0.323	0.829	0.350	4.383	3.719	0.485	0.0002	0.0014	0.2832
HOXA3	HOXB5	HOXB6	0.358	1.074	0.624	5.386	5.950	2.849	0.0002	0.0002	0.0062
HOXB8	HOXA2	HOXA7	0.258	0.704	0.704	3.529	3.351	3.908	0.0006	0.0014	0.0006
HOXB8	HOXB3	HOXB5	0.291	0.913	0.913	4.807	5.707	6.391	0.0002	0.0002	0.0002
HOXA1	HOXB3	HOXB6	0.254	0.715	0.715	4.076	4.118	4.722	0.0006	0.0010	0.0002
HOXB7	HOXB3	HOXB6	0.320	0.809	0.809	5.908	5.054	5.646	0.0002	0.0002	0.0002
HOXB7	HOXB3	HOXB5	0.275	0.786	0.786	4.365	4.544	5.126	0.0002	0.0002	0.0002
MEIS1	HOXA2	HOXA3	0.343	0.916	0.839	5.603	5.177	5.161	0.0002	0.0002	0.0002
HOXB8	HOXA2	HOXA3	0.326	0.869	0.820	5.187	4.799	4.961	0.0002	0.0002	0.0002
HOXA1	HOXA3	HOXA7	0.292	0.842	0.627	5.189	5.403	3.866	0.0002	0.0002	0.0004
HOXB8	HOXB5	HOXB6	0.296	0.872	0.872	4.051	4.394	5.032	0.0002	0.0002	0.0002
HOXB8	HOXB3	HOXB6	0.322	0.994	0.994	5.948	6.816	7.519	0.0002	0.0002	0.0002
MEIS1	HOXA2	HOXA5	0.367	0.935	0.888	6.605	5.764	5.985	0.0002	0.0002	0.0002
HOXA1	HOXA2	HOXA5	0.256	0.665	0.548	3.732	3.283	2.765	0.0002	0.0022	0.0102
NR2F2	GATA2	HOXA3	0.271	0.690	0.690	8.225	8.144	8.451	0.0002	0.0002	0.0002
MEIS1	HOXA2	HOXA7	0.266	0.664	0.632	3.780	3.049	3.276	0.0002	0.0040	0.0042

TABLE S1: The list of the 32 high-significant triples involving and new candidates for triadic interactions obtained by applying the Triaction algorithm to the AML gene-expression data.

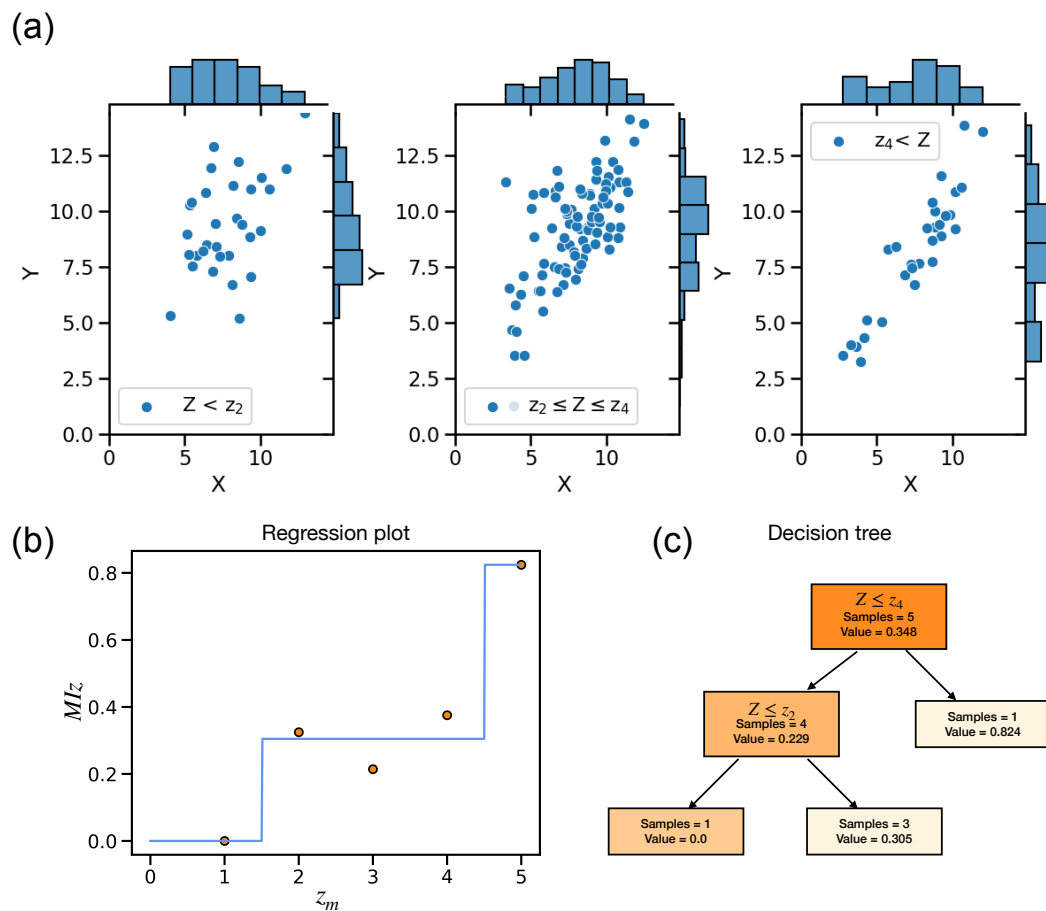


FIG. S6: **Strong triadic interaction:** We choose as thresholds the values defined by the tree to split the data (here z_2 and z_4). $X = \text{GATA1}$, $Y = \text{TAL1}$, $Z = \text{KLF5}$, $\Sigma = 0.27$, $\Theta_\Sigma = 3.07$, $P_\Sigma = 0.0038$, $T = 0.82$, $\Theta_T = 3.62$, $P_T = 0.0014$, $T_n = 0.45$, $\Theta_{T_n} = 1.19$, $P_{T_n} = 0.124$, $z_2 = 5.3$, $z_4 = 7.2$

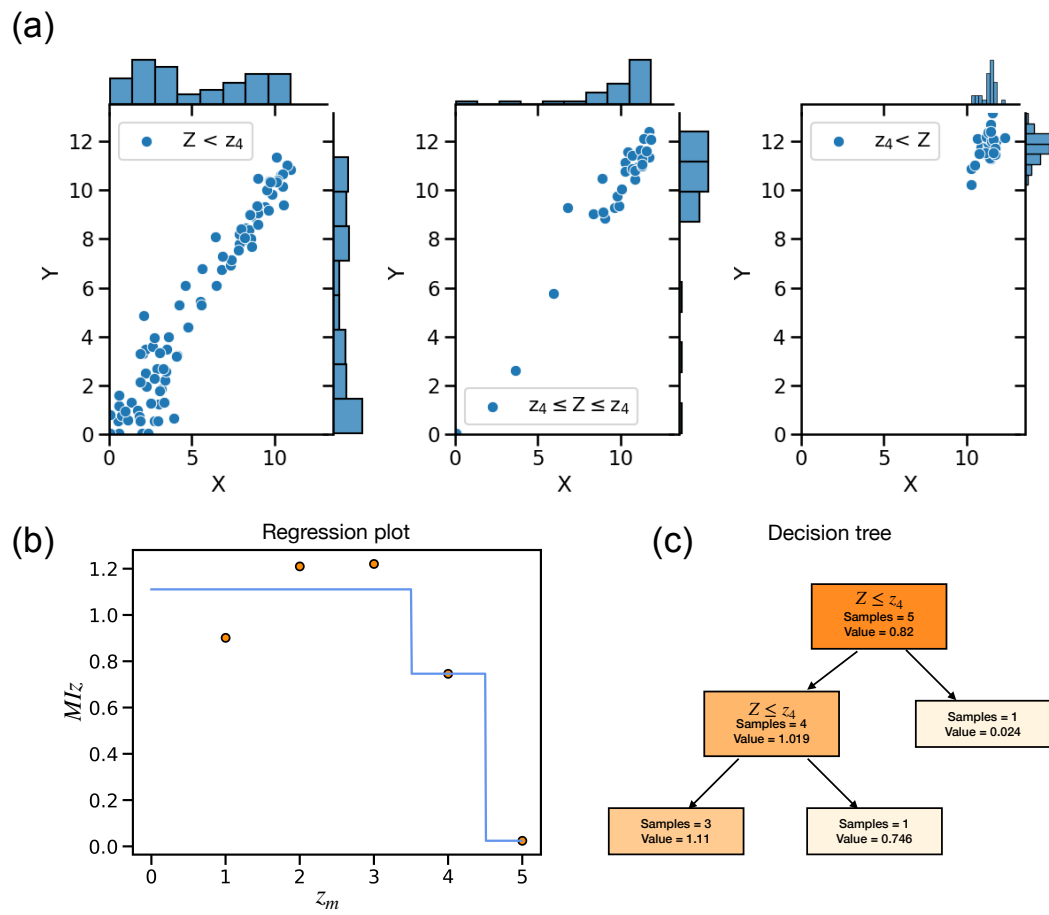


FIG. S7: **Strong triadic interaction:** We choose as threshold the value defined by the tree to split the data (z_4). $X = \text{HOXA3}$, $Y = \text{HOXA5}$, $Z = \text{PBX3}$, $\Sigma = 0.44$, $\Theta_\Sigma = 6.33$, $P_\Sigma = 0.0002$, $T = 1.20$, $\Theta_T = 6.07$, $P_T = 0.0002$, $T_n = 0.72$, $\Theta_{T_n} = 3.12$, $P_{T_n} = 0.0048$, $z_4 = 12.8$.

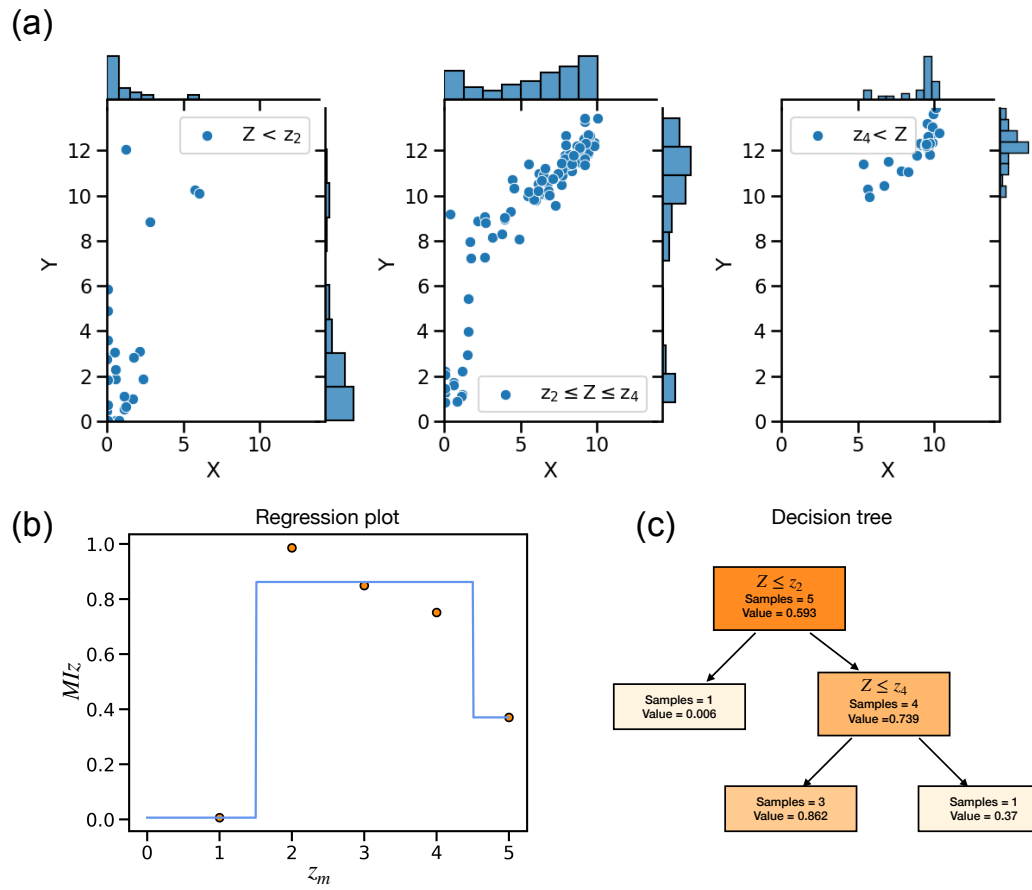


FIG. S8: **Strong triadic interaction:** We choose as thresholds the values defined by the tree to split the data (here z_2 and z_4). $X = \text{HOXA7}$, $Y = \text{HOXA9}$, $Z = \text{HOXA1}$, $\Sigma = 0.36$, $\Theta_\Sigma = 4.09$, $P_\Sigma = 0.0006$, $T = 0.98$, $\Theta_T = 3.93$, $P_T = 0.0006$, $T_n = 0.98$, $\Theta_{Tn} = 4.52$, $P_{Tn} = 0.0002$, $z_2 = 4.6$, $z_4 = 7.1$

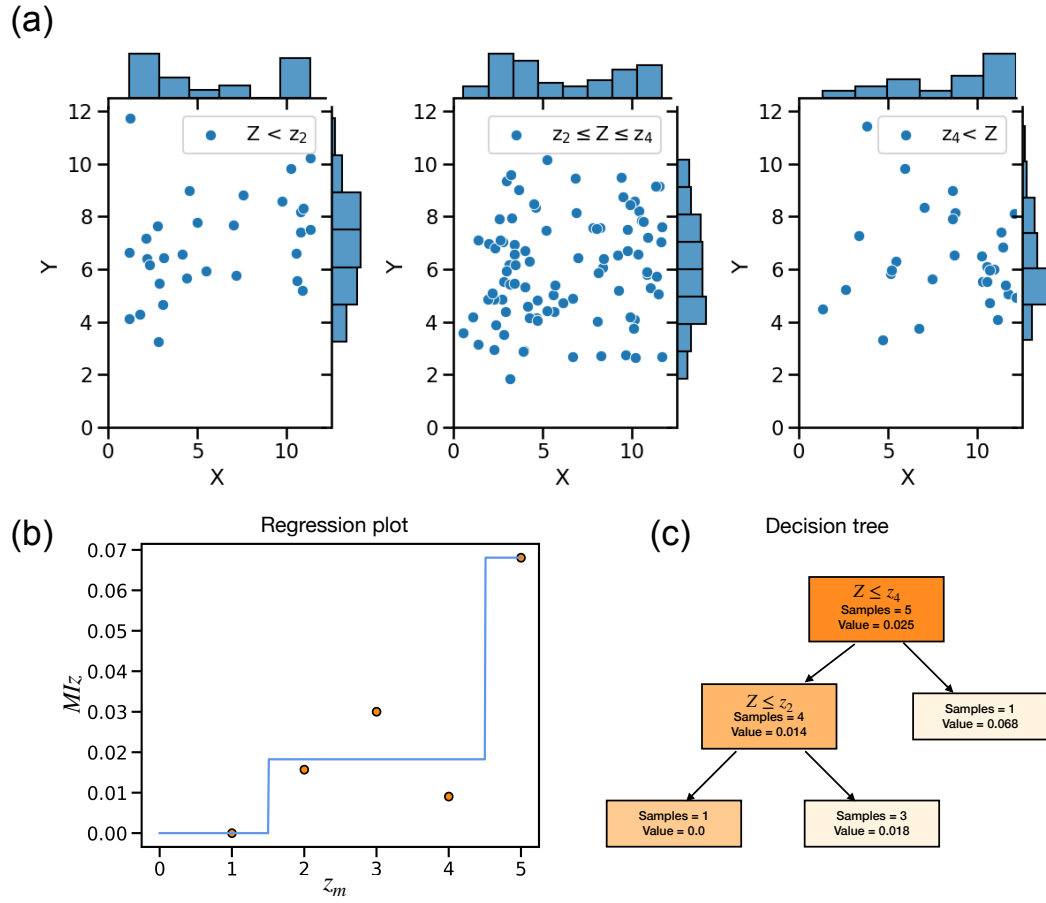


FIG. S9: **Non triadic interaction:** We choose as thresholds the values defined by the tree to split the data (here z_2 and z_4). $X = \text{AR}$, $Y = \text{NR4A3}$, $Z = \text{FLI1}$, $\Sigma = 0.024$, $\Theta_\Sigma = 0.99$, $p_\Sigma = 0.838$, $T = 0.068$, $\Theta_T = 0.88$, $p_T = 0.81$, $T_n = 0.059$, $\Theta_{Tn} = 0.91$, $P_{Tn} = 0.822$, $z_2 = 12.9$, $z_4 = 13.3$.